THE JOURNAL OF PHYSICAL CHEMISTRY C

ARTICLE

pubs.acs.org/JPCC

# UV-Raman and $^{29}$Si NMR Spectroscopy Investigation of the Nature of Silicate Oligomers Formed by Acid Catalyzed Hydrolysis and Polycondensation of Tetramethylorthosilicate

Anouschka Depla,[†] Elke Verheyen,[†] An Veyfeyken,[†] Marc Van Houteghem,[‡] Kristof Houthoofd,[†] Veronique Van Speybroeck,[‡] Michel Waroquier,[‡] Christine E. A. Kirschhock,[†] and Johan A. Martens*[,†]

[†]Center for Surface Chemistry and Catalysis, K.U. Leuven, Heverlee, Belgium

[‡]Center for Molecular Modeling, Ghent University, Zwijnaarde, Belgium

Supporting Information

**ABSTRACT:** Tetramethylorthosilicate (TMOS) was hydrolyzed and polymerized under strongly acidic conditions in the presence of substoichiometric quantities of water. The polymerization reaction was monitored during 64 h using $^{29}$Si NMR and UV-Raman spectroscopy. The nature of the oligomers and the condensation reaction pathways were unraveled using this combination of experimental techniques together with molecular modeling. $^{29}$Si NMR and UV-Raman signals which previously were not documented in literature could be assigned. TMOS rapidly was converted into short straight methoxylated silicate chains. Subsequently the growth of oligomers proceeded by condensations between a hydrolyzed middle group of a chain with an end-group of another chain. Larger oligomers were attached to each other via condensations between middle groups generating multiply branched structures. Rings were formed late in the reaction scheme through internal condensations of sizable silicate molecules. Oligomers that were characteristic of the different stages of the polymerization process were proposed. Oligomerization pathways starting from tetramethylorthosilicate and tetraethylorthosilicate (TEOS) are significantly different. While with TMOS rings are formed only late in the oligomerization scheme, with TEOS rings are formed at early stages through cyclo-dimerization. This insight into the different nature of the oligomers obtained from TMOS and TEOS will assist the design of new silica sol−gel materials.

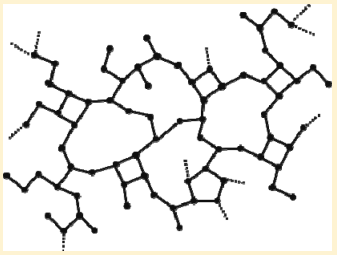

## INTRODUCTION

Silica sol−gel chemistry refers to the hydrolysis and condensation of a monomeric silicon alkoxide source in the presence of solvent and homogeneous catalyst into sol and gel. Many industrial manufacturing schemes of specialty silica materials including fibers, coatings, films, gels, glasses, and ceramics are based on silica sol−gel chemistry.[1−7] In sol−gel processes the properties of the final silica material are largely dependent on the nature of the silicate polymer and, especially, the formation of linear versus branched chains and ring structures. Crucial parameters of the silica sol−gel processes are the water:alkoxide molar hydrolysis ratio designated as the *r* value, the pH, the nature of the alkoxide, and the addition of organic solvent.[8−23] In general terms, high pH, and high *r* values favor the formation of highly branched silicate networks suited for manufacturing of colloidal silica or silica gel.[24−30] The use of a homogeneous acid catalyst leads to more linear polymer chains and is recommended when materials with low fractal dimension such as films and fibers are desired.[12]

Recent studies have shown that this traditional vision on the impact of the catalyst selection on branched versus linear polymer growth may be too simplistic. Insight into vibrational fingerprints revealed with UV-Raman spectroscopy of silicate oligomers is steadily growing.[31−46] Using $^{29}$Si NMR and small angle X-ray scattering, Brinker and Assink observed significantly branched silicate chains obtained under acidic conditions.[47] Further evidence for the presence of branched oligomers was provided by $^{29}$Si NMR and Raman spectroscopy.[12,17,48−51] In support of these observations, occurrence of cyclization reactions in acid catalyzed silica sol−gel processes has been detected.[12,17,48,49,52−59]

In an earlier publication we reported a similar investigation of acid catalyzed silica polymerization starting from tetraethylorthosilicate (TEOS) using $^{29}$Si NMR, UV-Raman, and molecular modeling.[60] The identity of oligomers formed at *r* values of 2 and lower could be identified and the reaction scheme projected. In the polymerization process departing from TEOS, linear chains no longer than hexamer are formed next to rings composed of three to six silicate units and branched specimen. The main reaction pathways in acid catalyzed silica oligomerization departing from TEOS are chain extension through monomer addition, formation of rings via cyclo-dimerization, and branchings through attachment of dimer and trimer.

Previously we noticed significant differences in the properties of silica gel obtained from TMOS and TEOS under almost

**Received:** January 19, 2011
**Revised:** May 5, 2011
**Published:** May 16, 2011

**Table 1. Overview of Samples**

| sample code | *r* value | TMOS (mL) | MeOH (mL) | $H_2SO_4$ (mL) | $H_2O$ (mL) | TMOS:$H_2O$:MeOH:$H_2SO_4$ molar ratio |
|---|---|---|---|---|---|---|
| R-0.1 | ~0.1 | 10.442 | 8.783 | 0.673 | 0.103 | 1:0.1:3.07:0.35 |
| R-0.9 | 0.9 | 10.183 | 8.565 | 0.656 | 0.597 | 1:0.9:3.07:0.35 |
| R-1.3 | 1.3 | 9.876 | 8.307 | 0.636 | 1.180 | 1:1.3:3.07:0.35 |

identical reaction conditions.[61,62] While the use of TEOS led to the formation of microporous silica gel, its substitution with TMOS led to the formation of mesoporous material.[61] A standing question was how the choice of alkoxide affected the oligomerization reaction scheme. In this work we unraveled the molecular aspects and underlying mechanism of the silica oligomerization process departing from TMOS. We applied the same methodology of combined UV-Raman and $^{29}$Si NMR, successfully applied on the TEOS sol−gel chemistry.[60] Raman frequencies and $^{29}$Si NMR chemical shifts have been computed for the different species using ab initio molecular modeling techniques. Significant differences in silicate speciation were observed, increasing the insight into the nature of the final silica gel materials that are obtained from TMOS versus TEOS.

## EXPERIMENTAL SECTION

In a typical sample preparation TMOS (Acros, 99%) and methanol (VWR, absolute grade, 99.9%) were mixed. Concentrated $H_2SO_4$ (Fisher, 98%) and optional water were added dropwise in this order under continuous stirring. The molar ratio of TMOS:MeOH:$H_2SO_4$ was 1:3.07:0.35. Water was added to reach a molar $H_2O$:TMOS ratio of 0.5 or 1.0 initially. After preparation in open recipients the samples were either sealed in polypropylene bottles (20 mL) for sample aging or transferred into NMR sample tubes, sealed, and introduced in the $^{29}$Si NMR instrument. The samples were hygroscopic and rapidly absorbed some water from ambient air. The actual *r* value was determined based on the hydrolysis and condensation state of the Si atoms determined by $^{29}$Si NMR sequences following a method explained in a previous publication.[60] In short, the *r* value was calculated from the number of hydrolyzed groups, assuming quantitative reaction of all water present. The *r* value for the samples with initial molar $H_2O$:TMOS ratio of 0.5 and 1.0 increased to 0.9 and 1.3, respectively. Specifically for the UV-Raman investigation a third sample with minimum water content was prepared (R-0.1). The chemical compositions of the samples R-0.1, R-0.9, and R-1.3 are given in Table 1.

Raman spectra were recorded using a Raman instrument combining of a Coherent Innova 300C MotoFred laser, a Roper Scientific Trivista TR557 A&S triple-stage spectrometer, and a CCD camera (Princeton Instruments). The spectrometer stages were equipped with 900−900−3600 grooves/mm grating combination. An excitation beamline at 244 nm wavelength with an output power of 10 mW was used. The silicate samples were analyzed in open shallow cylindrical vessels rotating horizontally. To minimize local heating, a short exposure time to the laser beam of 80 s was applied. Each spectrum was an average accumulation of three recordings, each on a fresh sample. Possible instrumental frequency shifts were corrected using PTFE as a shift reference. Spectra were normalized for intensity based on the 1455 cm$^{-1}$ vibration, assigned to the asymmetrical C−H bending of methoxide groups of both TMOS and MeOH. A Savitzky−Golay algorithm with a filter coefficient of 5 was applied to smooth the spectra.

$^{29}$Si NMR spectra of samples R-0.9 and R-1.3 were recorded on a Bruker Avance II+ 600 spectrometer (14.1 T). Samples (3 mL) were loaded in 10 mm quartz tubes. The spinning frequency was 16 Hz. Experimental conditions comprised a recycle delay of 80 s and pulse lengths of 12.0 ms (R-0.9) or 10.0 ms (R-1.3). These pulse lengths correspond to a tip angle of 90°. Recordings of samples R-0.9 and R-1.3 contained 65536 and 16384 time domain data points (td), respectively. Tetramethylsilane served as external chemical shift reference. Measurements were performed without lock, under isothermal conditions at 298 K. Shimming was performed on a solution of TMS-salt (trimethylsilylpropane sulfonic acid, Merck) in 3 mL of $D_2O$. Each acquisition in the time sequence represented an accumulation of 28 scans.

## THEORETICAL SECTION

All theoretical predictions for Raman vibrational frequencies Raman[63] and $^{29}$Si NMR chemical shifts[64] were derived from static quantum chemical methods using the Gaussian03 program.[65] Ab initio molecular dynamics simulations are the most natural way to reproduce IR and Raman spectra, but for larger oligomers they require a high computational cost as long simulation times are needed. Alternatively, classical molecular dynamics methods make calculations feasible but require adequate force fields. For Raman spectra the Fourier transform of the autocorrelation function of the time variation of the electric polarizability matrix should be evaluated from the trajectories. This is very sensitive to the applied force field, and for the specific purpose of this paper we have preferred the static approach.[66] All chain structures from monomer up to octamer and some cyclosilicates (three- and four-rings) were optimized in vacuo at the B3LYP/6-31+g(d) level of theory.[67] This level of theory has been recognized as one of the best performing functionals for geometry optimizations and has already been used in previous studies on silica oligomerization.[29,60] DFT based harmonic vibrational frequencies are normally scaled to compare with experimental values. The scale factor is uniform for a given level of theory[68] and has been determined via an optimal correlation between theoretical and experimental values for all structures ranging from monomer up to pentamer (see Supporting Information). This scale factor amounts to 1.0335 for Raman frequencies and is in good agreement with theoretically determined scale factors proposed by Radom et al.[68] for low frequencies. The model assumes all species fully saturated with methoxide groups, justified at low molar hydrolysis ratio. The configurational dependency of the spectra was verified by considering different conformers for each species. For all species a large number of conformers was investigated ranging from linear to curled up conformers and various internal rotations were applied to scan for a large variety of structures. From these structures we have selected the most stable ones differing in binding energy by no more than 5 kJ mol$^{-1}$. The coordinates of all selected conformers are given in the Supporting Information. Vibrational frequencies for all conformers have been computed, yielding mean values and widths. Maximal variation between conformers appeared to be ~20 cm$^{-1}$.

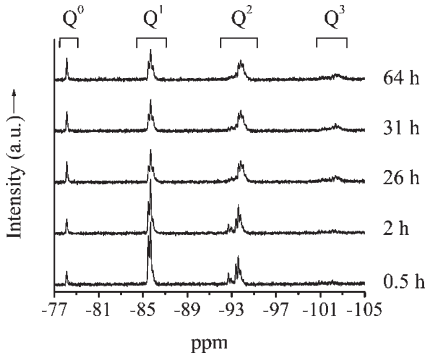


**Figure 1.** $^{29}$Si NMR spectra of the polycondensation process of R-0.9 sample.

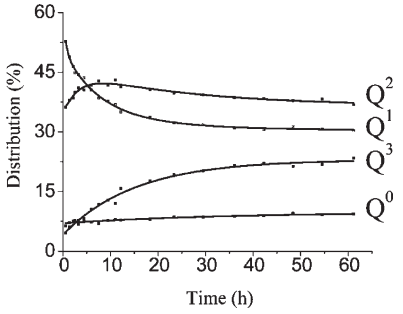


**Figure 2.** $Q^n$ distribution in R-0.9 sample according to $^{29}$Si NMR against time.

For $^{29}$Si NMR, chemical shifts were calculated for all silicon atoms of the structures mentioned above and averaged out over $Q^0$, $Q^1$, $Q^2$, and $Q^3$ sites. A distinction was made between $Q^2$ species in chains and $Q^2$ species in rings. Single-point calculations with a triple-$\zeta$ basis set 6-311++g(d,p) were performed on B3LYP/6-31+g(d) optimized geometries for the $^{29}$Si NMR signals.[69] Solvent effects on NMR shifts are well-known and have been investigated to some extent on nitrogen shielding constants.[70] Most of the previous ab initio calculations of chemical shifts on small silica species have ignored the effect of the molecular environment.[71] Recently some studies included these effects either by using an implicit solvent model[72] or by adding some discrete solvent molecules to the silica clusters.[73] The silica clusters under consideration in this paper are relatively large, ranging from 20 to about 120 atoms. Explicitly solvating these clusters with solvent molecules is not feasible as it would require a lot of explicit solvent molecules.[74] Moreover, the position of each of these solvent species would have to be equilibrated by means of molecular dynamics simulations.[75] To account for the solvent environment, we used a scale factor for the NMR shifts by determining an optimal correlation between theoretical and experimental values for the $Q^0$, $Q^1$, $Q^2$, and $Q^3$ sites (See Supporting Information). The scale factor was determined as 0.9596.

## RESULTS AND DISCUSSION

**Identification of Silicate Oligomers Using $^{29}$Si NMR, UV-Raman, and Molecular Modeling.** Our samples prepared from TMOS at low $r$ values in strongly acidic conditions were homogeneous and suitable for $^{29}$Si NMR spectroscopy. The R-0.9 sample was prepared and loaded into the NMR apparatus. About 70 $^{29}$Si NMR spectra were taken in the period from 0.5 to 64 h. Chemical shifts of specific signals were determined in the 70 spectra and averaged. For the majority of signals the accuracy of the chemical shift was within 0.01 ppm. Examples of spectra recorded 0.5, 2, 26, 31, and 64 h after preparing the sample are shown in Figure 1. The spectra comprised signals of $Q^0$, $Q^1$, $Q^2$, and $Q^3$ silicate connectivities, the subscript in the Q symbol referring to the number of siloxane bonds of the Si atom. The evolution of the distribution of $Q^n$ environments in R-0.9 sample according to $^{29}$Si NMR is presented in Figure 2. The $Q^0$ signal was constant and represented less than 10% of all silicon atoms. End groups ($Q^1$) were dominant in the first hours (Figure 2). A formation of dimers and short chains can account for such high content of end groups. The $Q^1$ concentration decreased from over 50% initially to a final level of ca. 30% of the Si atoms. Si atoms in chains linked to two Si atoms via siloxane bridges ($Q^2$) were present all the time. Their concentration reached a maximum after ca. 6 h. The content of branchings ($Q^3$) originally was very low but steadily increased all along the investigated 64 h period. The concentration of fully condensed Si atoms ($Q^4$) remained below the detection limit. At this low water content and high acidity the network cannot reach a high level of connectivity within the monitored time frame.

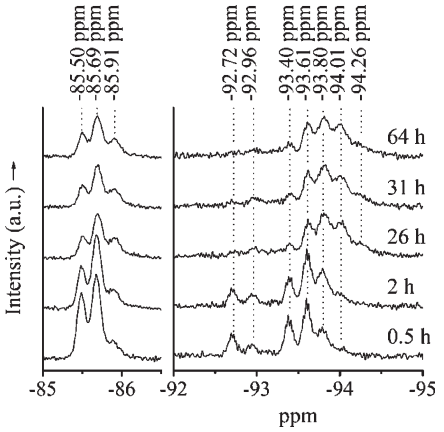


**Figure 3.** Detail of $Q^1$ (left) and $Q^2$ (right) range of $^{29}$Si NMR spectra of Figure 1.

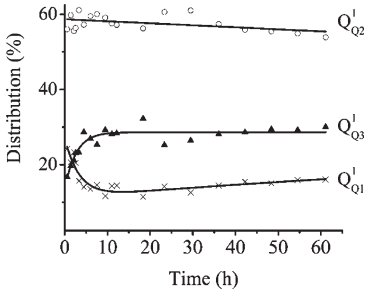


**Figure 4.** Distribution of $Q^1$ $^{29}$Si NMR signals in R-0.9 sample against aging time. Lines are meant to guide the eye.

Details of the $^{29}$Si NMR spectra of Figure 1 in the $Q^1$ and $Q^2$ regions are provided in Figure 3. One signal was observed in the $Q^0$ range, assigned to TMOS ($Q^0$, $\delta$ = −78.14 ppm, Figure 1). The $Q^1$ region showed three well-resolved signals (Figure 3). Next to the $Q^1$ signal assigned to dimer ($Q^1_{Q1}$, $\delta$ = −85.50 ppm),[48−51,54] two additional $Q^1$ signals were observed at $\delta$ = −85.69 and −85.91 ppm. Si atoms terminating chains of trimers and longer chains


dx.doi.org/10.1021/jp200568j |J. Phys. Chem. C 2011, 115, 11077–11088

typically show a resonance around −85.7 ppm,[48,54,76] leading to the assignment of the signal at −85.69 ppm to $Q^1$ end groups connected to a $Q^2$ and denoted $Q^1_{Q2}$. The third $Q^1$ signal at $\delta = -85.91$ ppm has hardly been discussed in the literature.[48] From the evolution of the internal distribution of $Q^1$ signals (Figure 4) it appeared that the species associated with the −85.91 ppm signal were formed later than dimer and chains. The $\delta = -85.91$ ppm signal grew in parallel with the signals in the $Q^3$ range. This led to a tentative assignment of the −85.91 ppm resonance to $Q^1$ end groups connected to a $Q^3$ silicon, denoted $Q^1_{Q3}$. On the basis of their chemical shift all $Q^1$ groups were methoxylated.

The $^{29}$Si NMR spectra in the $Q^2$ range showed eight resolved peaks (Figure 3). The assignment of the signals at −93.40, −93.61, and −93.80 ppm to $Q^2$ Si atoms of linear fully methoxylated trimer, tetramer and pentamer was based on the literature.[48−51,54,76] These three signals dominated the $Q^2$ range after 0.5 and 2 h. After 26 h and later two additional upfield signals gained intensity with maximum intensity around −94.01 and −94.26 ppm, respectively (Figure 3). These signals have not been documented before. Their position and gain in intensity at later stages of the experiment led to a tentative assignment to $Q^2$ middle atoms of chains containing more than five Si atoms, i.e., chains of six Si (−94.01 ppm) and seven Si units (−94.26 ppm), respectively. The presence of a shoulder upfield of the −94.26 ppm signal hints at the formation of even longer chains.

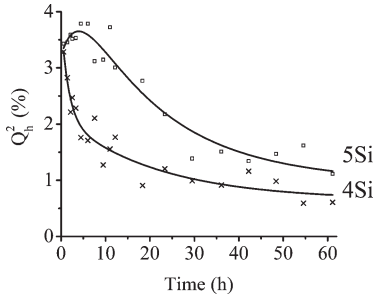


**Figure 5.** Content of hydrolyzed $Q^2_h$ groups in chains with 4Si, 5Si, and 6 or more Si atoms (6Si+) according to $^{29}$Si NMR against time during the polycondensation of sample R-0.9. Lines are meant to guide the eye.

The five already discussed $Q^2$ signals were assigned to fully methoxylated molecules. In the $Q^2$ range the first two $^{29}$Si NMR spectra (0.5 and 2 h) showed additional signals downfield of the signals of fully methoxylated molecules at $\delta = -92.72$, −92.96, and −93.2 ppm, respectively (Figure 3). Due to the low intensity the last signal will not be quantitatively interpreted. Signals in this chemical shift region have been assigned in literature either to $Q^2$ signals of cyclosilicates or to chains containing one hydrolyzed $Q^2$ silicon.[48−50,54,76] Brunet et al.[48] observed $^{29}$Si NMR signals at chemical shifts similar to those presently observed and assigned them to $Q^2$ silicons of branched 4-rings. Kelts and Armstrong observed similar spectra in an acid catalyzed TMOS oligomerization and originally assigned them to hydrolyzed linear groups.[50] In a later study in which TMOS and TEOS hydrolysis and condensation were compared, those authors modified their interpretation of the discussed signals in favor of cyclosilicates.[49] In the present study the intensity of the signals at $\delta = -92.72$ and −92.96 decreased strongly in the period from 2 to 26 h (Figure 3). Provided the assignments to cylcosilicates were correct, these $Q^2$ silicons either would have been converted to $Q^3$ via the formation of branchings or else to $Q^2$ and $Q^1$ groups of chains via a break-up of these rings. According to Brunet et al.[48] the $Q^3$ signature of ring Si atoms carrying a branching are to be found at $\delta \sim -101$ ppm. In our experiment, $Q^3$ signals in the region around −101 ppm were weak in early NMR spectra and decreased rather than increased in intensity when the discussed $Q^2$ signals weakened. Only weak signals assigned to $Q^3$ environments were observed in the region −100 to −103 ppm (Figure 1) indicating the existence of silicate rings early in the synthesis was unlikely.

An alternative interpretation of the $Q^2$ signals at $\delta = -92.72$, −92.96, and −93.2 ppm was assumption of the presence of a hydrolyzed group on $Q^2$ Si atoms in chains. The presence of a hydrolyzed group in a chain has been reported to cause a downfield shift of ca. 0.9 ppm[50] or ca. 1.3 ppm[48,54,76] compared to the nonhydrolyzed oligomer. Compared with the chemical shifts of the $Q^2$ signals of fully methoxy terminated tetramer ($\delta = -93.61$ ppm), pentamer ($\delta = -93.80$ ppm), and hexamer ($Q^2$, $\delta = -94.01$) each of

**Table 2. Experimental and Theoretical $^{29}$Si-NMR Chemical Shifts**

| | | experimental $^{29}$Si NMR signal (ppm) | | |
|---|---|---|---|---|
| $Q^i$ region | species | R-0.9[a] | R-1.3 | theoretical region (ppm)[b] |
| $Q^0$ | monomer | −78.14 | | −74.97; −77.16 |
| $Q^1$ | | | | −82.78; −88.36 |
| $Q^1_{Q1}$ | dimer | −85.50 | −85.5 | |
| $Q^1_{Q2}$ | end-group of $Q^2$ | −85.69 | −85.7 | |
| $Q^1_{Q3}$ | end-group of $Q^3$ | −85.91 | −85.9 | |
| $Q^2$ | | | | −90.96; −99.65 |
| | 3Si | −93.40 | −93.4 | |
| | 4Si | −93.61 | −93.6 | |
| | 5Si | −93.80 | −93.8 | |
| | 6Si$^+$ | −94.01; −94.26 | −94.0; −94.3 | |
| $Q^2$ hydr. | | −92.72; −92.96; −93.2 | −92.4; −92.7; −93; −93.2 | |
| $Q^3$ | branches | [−100; −103] | [−99.5; −103.5] | −92.84; −105.38 |

[a] Chemical shifts of specific signals have been determined and averaged over about 70 $^{29}$Si NMR spectra. The error margin on the experimental $^{29}$Si NMR signal (ppm) for R-0.9 was 0.01 for all fully methoxide terminated species and 0.03 for the hydrolyzed specimen. [b] Theoretical values were scaled with a factor of 0.9596, determined by the optimal correlation between the theoretical and experimental values for the $Q^0$, $Q^1$, $Q^2$, and $Q^3$ environments (see Supporting Information).

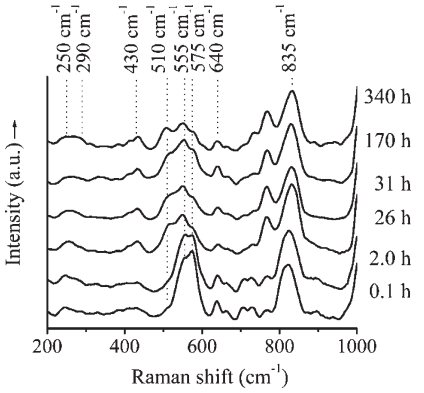


**Figure 6.** UV-Raman spectra of the condensation process of R-0.9 sample.

the signals at $\delta$ = −92.72, −92.96, and −93.20 ppm $Q^2$ exactly present this downfield shift by ~0.9 ppm. According to this assignment, in the $^{29}$Si NMR spectra after 0.5 and 2 h, $Q^2$ groups in tetramers were most abundant (signals at −92.72 ppm for tetramer with hydrolyzed group and −93.61 ppm for unhydrolyzed tetramer, respectively). The content of hydrolyzed $Q^2$ groups in chains with four and five Si atoms was plotted against time in Figure 5. In the first hours, the content of hydrolyzed $Q^2$ groups in 4Si chains rapidly decreased, while later hydrolyzed groups in chains with 5Si atoms dominated among the hydrolyzed $Q^2$ groups.

Linear trimer hydrolyzed at $Q^2$ was expected to cause a $Q^2$ $^{29}$Si NMR signal around −92.50 ppm considering a downfield shifting by 0.9 ppm of the −93.40 ppm signal assigned to fully methoxylated trimer. However, at the expected chemical shift no peak was observed (Figure 3). Similarly, in the $Q^0$ and $Q^1$ range the $^{29}$Si NMR spectra did not show any signal that could be assigned to hydrolyzed species (Figure 1). The concentration of hydrolyzed monomer, dimer, trimer, and of end groups of chains was low in this TMOS system. These groups apparently were short-lived and their concentration was therefore below the detection limit during the first $^{29}$Si NMR recording. Apparently, hydrolyzed groups persisted only on $Q^2$ silicons in chains with four and more Si atoms.

In the time sequence of $^{29}$NMR spectra (Figure 1) relatively weak $Q^3$ signals were observed. Systematic investigation of the 70 collected spectra revealed intensity maxima occurred at $\delta$ = −100.9, −101.15, −101.45, and −101.8 ppm at early times. With time, $Q^3$ signals at more negative chemical shifts of −102.08, −102.35, and −102.6 ppm were detected. A listing of $^{29}$Si NMR signals and their assignment in the R-0.9 sample is provided in Table 2.

Raman spectra of sample R-0.9 during its evolution are presented in Figure 6. The TMOS monomer was responsible for a Raman signal at ~640 cm$^{-1}$. Raman signals of dimer and end groups of chains coincided around 575 cm$^{-1}$.[16,17,51,60,77] Molecular modeling confirmed these assignments (Table 3). The representative silica structures are shown in Figure 7. The Raman active band at 575 cm$^{-1}$ corresponds to a global stretching vibration. The frequency of the maximum of the band depended on the relative concentration of the dimer versus end groups. In UV-Raman spectra of sample R-0.9 the signal at ~575 cm$^{-1}$ was in the lower range of the wavenumbers reported for this signal in literature pointing at dominating dimers. In the time series of Raman spectra, the ~575 cm$^{-1}$ band decreased in intensity in favor of

**Table 3. Experimental and Theoretical Raman Shifts**

| species | experimental shift (cm$^{-1}$) | theoretical shift region (cm$^{-1}$) |
|---|---|---|
| monomer | 640 | [ 639−649 ] |
| dimer (+end groups) | 575 | [ 568−578 ] |
| 3Si | 555 | [ 543−553 ] |
| 4Si | ~540 | [ 522−542 ] |
| 5Si | 510 | [ 515−535 ] |
| 6Si | | [ 515−535] |
| 7Si | | [ 515−535 ] |

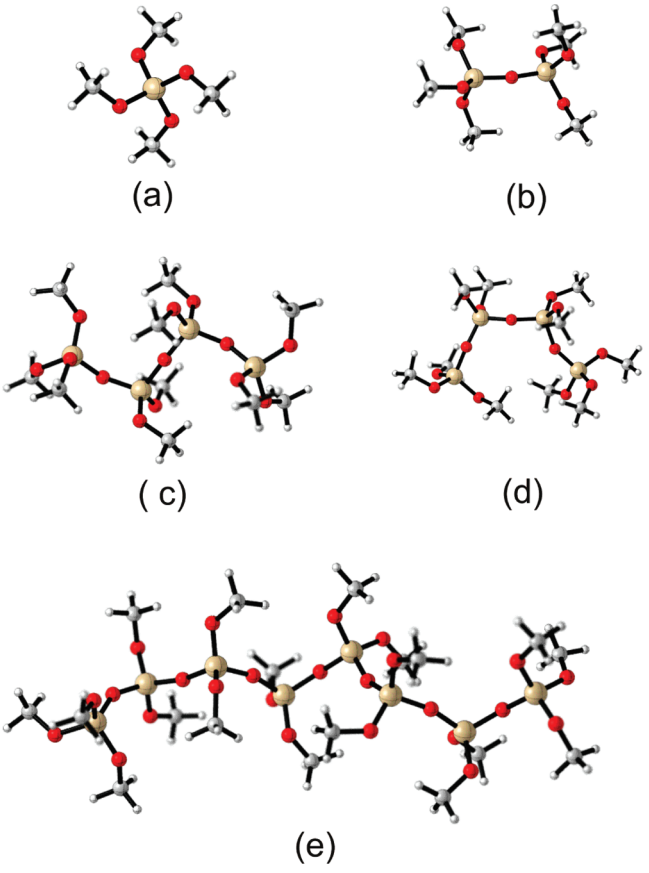


**Figure 7.** Some of the lowest energy conformers of monomer (a), dimer (b), tetramer (open (c) and closed (d) configuration), and octamer (e).

signals at ~555 and ~510 cm$^{-1}$. The latter two vibrations could not be readily assigned. From $^{29}$Si NMR spectra (Figure 3) it was known that linear trimers, tetramers, and pentamers were dominant. Literature reports the vibrations of linear trimer and tetramer at wavenumbers of 525 and 484 cm$^{-1}$, respectively.[16,51] Absorptions at such wavenumbers were absent in the Raman spectra of the R-0.9 sample. According to ab initio modeling, trimer, tetramer, and pentamer vibrations were to be expected in the regions of 543−553, 522−542, and 515−535 cm$^{-1}$, respectively. On the basis of these models, the experimentally observed Raman band around 510 cm$^{-1}$ was attributed to pentamer. The assignment of the Raman band at 550−555 cm$^{-1}$ was less obvious and required

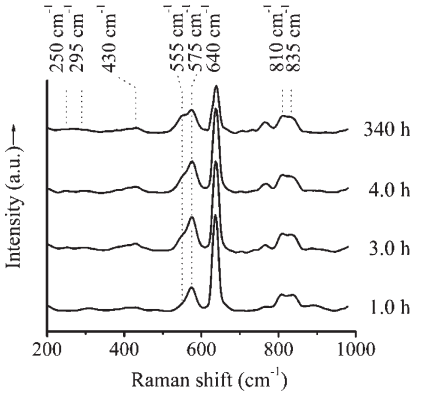


**Figure 8.** UV-Raman spectra of the condensation process of R-0.1 sample.

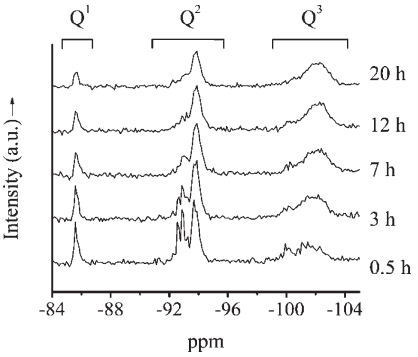


**Figure 9.** $^{29}$Si NMR spectra of the condensation process of R-1.3 sample.

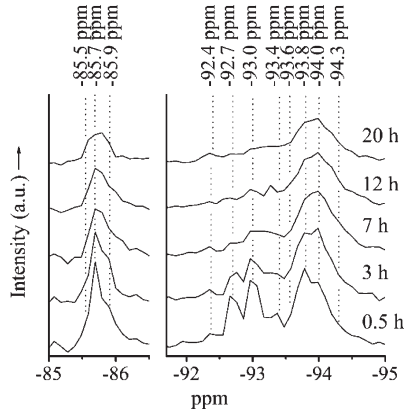


**Figure 10.** Detail of $Q^1$ range (left) and $Q^2$ range (right) of the $^{29}$Si NMR spectra of Figure 9.

further investigation. A sample with very low $r$ value (R-0.1) was prepared in order to further limit the extent of oligomerization. In this sample the Raman signatures of monomer (~640 cm$^{-1}$) and dimer (~575 cm$^{-1}$) were prominent (Figure 8). A shoulder was present on the peak at ~575 cm$^{-1}$ which developed into a distinct vibration at ~555 cm$^{-1}$. The band at ~510 cm$^{-1}$ observed in the R-0.9 sample was absent. On the basis of these spectra and the molecular modeling locating trimer vibrations to the 543−553 cm$^{-1}$ range, the ~555 cm$^{-1}$ vibration was assigned to linear trimers. The Raman spectra of sample R-0.9 (Figure 6) revealed a gradual transformation of dimer (~575 cm$^{-1}$) and linear trimer (~ 555 cm$^{-1}$) into linear pentamer (~510 cm$^{-1}$) in agreement with NMR. The Raman signal of linear tetramers according to NMR also present in this sample presumably was contained in the envelope of ~510 and ~555 cm$^{-1}$ peaks (Figure 6). According to ab initio modeling, tetramers indeed were to be expected in the region of 522−542 cm$^{-1}$. A closer inspection revealed the maximum of the peak at ~555 cm$^{-1}$ shifted to 550 cm$^{-1}$ hinting tetramer contribution increased with time. Tetramer vibration has tentatively been assigned to be located around ~540 cm$^{-1}$. $^{29}$Si NMR of R-0.9 sample revealed the formation of 6Si and longer chains. According to our theoretical calculations, discrimination between Raman signatures of pentamers and longer linear chains was expected to be difficult (Table 3). The Raman bands of linear chains containing more than five Si atoms were expected in the region of 515−535 cm$^{-1}$, identical to the region of pentamers (Table 3). Thus Raman spectroscopy was less convenient for discriminating between longer chains. Hence, the broad band observed at ~510 cm$^{-1}$ was assumed to contain contributions from pentamers as well as from longer chains.

The Raman signals at ~810 and ~835 cm$^{-1}$ comprised the asymmetrical Si−O stretch (810 cm$^{-1}$) and the $CH_3$-rocking mode (835 cm$^{-1}$).[17,78] Raman bands at ~250, ~ 295, and ~430 cm$^{-1}$ in TMOS oligomerization hardly have been addressed in literature. The presence of these bands has been found to be highly dependent on the type of mineral acid, and they were estimated to be less relevant to the present analysis of oligomerization pathways. Vibrations at ~665, ~710, ~730, and ~770 cm$^{-1}$ observed in the R-0.9 sample occurred in a region usually assigned to hydrolyzed species.[13,16,17,24,51] Hydrolysis of methoxy groups lowers the molecular mass and was expected to cause the vibrations to shift toward higher wavenumbers. However, the R-0.1 sample with minimum water content displayed similar signals (Figure 8) making assignment of the vibrations at ~665, ~710, ~730, and ~770 cm$^{-1}$ to hydrolyzed species unlikely. Most probably is the vibration at ~770 cm$^{-1}$ associated with −$OCH_3$ and the evolution of a network with increasing connectivity. This is supported by the absence of this vibration in TEOS systems[60] and the strength of the signal observed in a fresh gel of the R-1.3 sample (vide infra) which contains still a large amount of $Q^2$ and $Q^3$ (see Supporting Information). Assignment of this signal to monomeric silica appears highly unlikely as $^{29}$Si NMR clearly indicates no such species are present. However the assignment of the vibrations at ~665, ~710, ~730, and ~770 cm$^{-1}$ remains elusive.

Further confirmation of the assignments of $^{29}$Si NMR and Raman signals in the R-0.9 sample was obtained by comparison to a sample with slightly higher molar hydrolysis ratio. $^{29}$Si NMR spectra of the R-1.3 sample are shown in Figure 9 with details in Figure 10. These $^{29}$Si NMR spectra were less resolved compared to the R-0.9 sample due to a lower number of data points in the time domain (cf. Experimental Section). Furthermore, in this sample with more advanced hydrolysis a distribution of chemical shifts has to be expected which also contributed to the observed line broadening. In this sample no $^{29}$Si NMR signal in the $Q^0$ range was discernible, revealing all TMOS had reacted. The $^{29}$Si NMR spectra recorded in the period 0.5−20 h indicated dominance of $Q^2$ and $Q^3$ environments (Figure 11). The $Q^3$ content steadily increased at the expense of $Q^2$. The number of $Q^1$ species remained almost constant.

The spectral features in the $Q^1$ and $Q^2$ range observed in the R-0.9 sample were also encountered in R-1.3. In the $Q^1$ range an

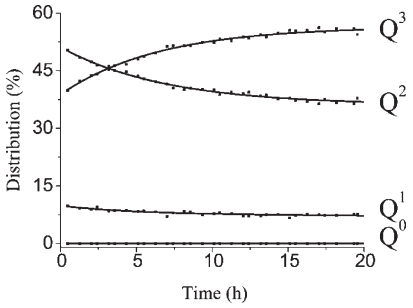


**Figure 11.** Evolution of Q distribution according to $^{29}$Si NMR in R-1.3 sample.

unresolved signal covered the signals of dimer (−85.5 ppm) and end groups of chains with more than 2Si atoms (−85.7 and −85.9 ppm). In the $Q^2$ range the $^{29}$Si NMR spectrum comprised signals of Si atoms of linear chains with one hydrolyzed group and fully methoxylated chains. Signals that could be ascribed to cyclosilicates were absent. In the $Q^2$ range the homologous series of methoxylated chains containing 3Si (−93.4 ppm), 4Si (−93.6 ppm), 5Si (−93.8 ppm), 6Si (−94.0 ppm), and even more Si (a signal assigned to −94.3 ppm) was observed. The $Q^2$ signal of 5Si (−93.8 ppm) dominated after 0.5 h, while after 20 h, the most intense $Q^2$ signal was assigned to 6Si (−94.0 ppm). Thus, the linear oligomers grew on average about one silicate unit longer than in R-0.9, where the pentamer signal (−93,8 ppm) dominated in the spectra after 26, 31, and 64 h (Figure 3). As before, chains with hydrolyzed methoxy groups at $Q^2$ positions were present in R-1.3 sample. The signals around −92.7 and −93.0 ppm were assigned to hydrolyzed tetramer and pentamer, respectively. In the R-1.3 sample the signal of pentamer, hydrolyzed at $Q^2$, dominated the signals of hydrolyzed species after 0.5 h (Figure 10), while in the R-0.9 sample the tetramer was dominant (Figure 3). The signal at −92.4 ppm was assigned to hydrolyzed $Q^2$ in trimer. Whereas this signal was absent in R-0.9, in the R-1.3 sample with slightly higher water content the trimer was partially hydrolyzed at $Q^2$. Similar to R-0.9 the $^{29}$Si NMR spectra of R-1.3 indicated no hydrolysis of end groups. The most significant difference between R-0.9 and R-1.3 samples was the higher relative intensity of $Q^3$ signals (region $\delta$ = −99.5 to −103.5 ppm) in R-1.3 (Figure 1 compared to Figure 9). A listing of $^{29}$Si NMR signals in R-1.3, their assignment, and a comparison with R-0.9 are provided in Table 2.

In the UV-Raman spectra of sample R-1.3 the most prominent signal relevant to silicate speciation was at ∼510 cm$^{-1}$ (Figure 12) confirming the abundant presence of pentamers and longer chains, in agreement with $^{29}$Si NMR. Increasing cross-linking and network formation causes a change in Si−O−Si bond length and angle. These alterations may lead to a shift of the vibrational frequency. The maximum of the band at ∼510 cm$^{-1}$ gradually shifted after 0.5 h to ∼500 cm$^{-1}$ after 3 h and to 490 cm$^{-1}$ after 20 h. In the R-1.3 sample the dimer signal (∼575 cm$^{-1}$) and the trimer and tetramer signals (∼550 cm$^{-1}$) were rather weak.

**Reaction Pathways of Acid Catalyzed TMOS Polymerization at Low *r* Value.** The detailed assignment of the silicate species obtained in acid catalyzed silica polymerization at low *r* value presented in the previous section allowed a detailed description of the reaction pathways. The first $^{29}$Si NMR spectrum was recorded 30 min after preparing the R-0.9 sample.

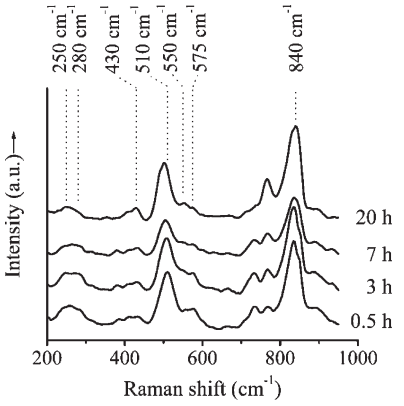


**Figure 12.** UV-Raman spectra of the condensation process of R-1.3.

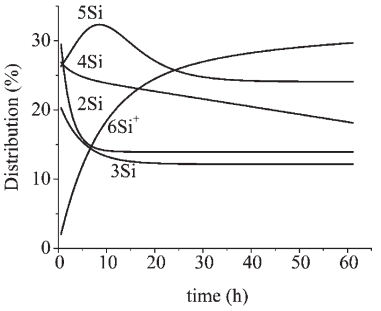


**Figure 13.** Evolution of the molar distribution (%) of silicate chain lengths in R-0.9 sample. Experimental data points were left out for clarity.

Less than 10% of all the added TMOS remained after 30 min. Apparently, in the first minutes, which for practical reasons could not be investigated, the reactions went rapidly. Hydrolysis is an acid catalyzed reaction. In acid catalyzed silica oligomerization departing from TMOS with substoichiometric quantities of water is a nucleophilic substitution reaction with a hydrolyzed Si−OH group acting as nucleophile and methoxy as a leaving group

$$\text{Si}-\text{OH} + \text{CH}_3-\text{O}-\text{Si} \rightarrow \text{Si}-\text{O}-\text{Si} + \text{MeOH}$$

Under the described conditions the methoxy group will be protonated, facilitating elimination. The *r* value of 0.9 estimated from the content of siloxane and hydrolyzed groups (Figure 2 and Figure 5) was in agreement with a conversion level of TMOS of around 90%. This consistency meant that very few water molecules were left unreacted in the sample.

With the recorded $^{29}$Si NMR spectra $Q^2$ environments in differently sized chains were separately detected and quantified (Figure 10 and Table 2). Dimers could be quantified based on their $Q^1$ signal. With this information, the evolution of the distribution of differently sized silicate chains was calculated and is shown in Figure 13. The figure with experimental data points is given in the Supporting Information. Note that in this estimation the contribution of $Q^3$ silicons to chains was neglected. Information on the distribution of $Q^3$ silicons over differently sized chains could not be unambiguously separated.

In the first hours, the content of dimers (2Si) in R-0.9 decreased rapidly from ca. 30 mol % after 30 min to ca. 12% after 20 h. Initially present 3Si and 4Si chains disappeared in favor


dx.doi.org/10.1021/jp200568j |*J. Phys. Chem. C* 2011, 115, 11077–11088

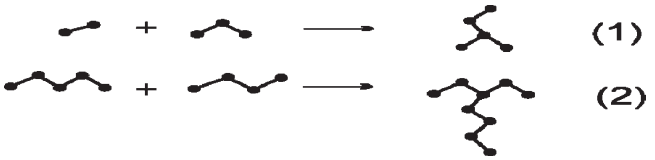


**Figure 14.** Examples of chain extension via condensation reactions between $Q^1$ and $Q^2$ groups. In reaction 1, dimer reacts with trimer into branched $Si_5$ oligomer; in reaction 2 tetramer and pentamer react together into branched $Si_9$ oligomer.

**Table 4. Representative Silicate Oligomers of Acid Catalyzed TMOS Polycondensation**

| | | Q ratio[a] | | | | |
|---|---|---|---|---|---|---|
| sample | time (h) | $Q^1_{Q3}$ | $Q^1_{Q2}$ | $Q^2$ | $Q^3$ | representative structure[b] |
| R-0.9 | 0.5 | 2 | 6.4 | 6.8 | 1 | model A |
| | 6 | 1 | 2.3 | 4 | 1 | model B |
| | 57 | 0.4 | 0.7 | 1.7 | 1 | model D |
| R-1.3 | 0.5 | | 0.24[c] | 1.26 | 1 | model E |
| | 20 | | 0.13[c] | 0.7 | 1 | model F |

[a] $Q^1_{Q2}$ and $Q^1_{Q3}$ represent $Q^1$ signals next to $Q^2$ and $Q^3$, respectively. [b] Presented in Figure 16. [c] $Q^1_{Q2} + Q^1_{Q3}$.

of chains with five and more Si atoms. The content of 5Si chains reached a maximum around 10 h. Later, chains with six and more Si atoms became dominant. Chain growth was not fed by monomer, since the monomer concentration remained constant. Although end-on condensation of short chains could account for part of the growth, the steady increase of the $Q^3$ content (Figure 2) revealed the importance of another type of growth proceeding via condensation reactions between $Q^1$ and $Q^2$ groups.

According to NMR, after 30 min reaction, hydrolyzed groups at $Q^2$ in silicon chains with four or more Si atoms were available for condensation reactions (Figure 3 and Figure 5). The majority of hydrolyzed groups at $Q^1$ silicons must have been more reactive and converted before the recording of the first $^{29}$Si NMR spectrum.

Two examples of condensation reactions involving $Q^1$ and $Q^2$ are visualized in Figure 14. Addition of a dimer to the central Si atom of a trimer leads to the formation of a branched $Si_5$ molecule with a main chain composed of 4Si atoms (Figure 14). The condensation of a pentamer via a $Q^2$ group with a tetramer via a $Q^1$ group leads to a $Si_9$ oligomer with a main chain composed of 7Si atoms and a 2Si side chain. Such processes can explain the observed chain extension (Figure 13) in parallel with an increase of branchiness (Figure 2). An important consequence of this interpretation is that the chain lengths to which the $^{29}$Si NMR and UV-Raman signals were assigned (Table 2 and Table 3) represent linear chains as well as main chains of branched oligomers.

The quantification of Si groups composing oligomers based on $^{29}$Si NMR led us to propose representative oligomers at different stages of the aging of sample R-0.9 (Table 4 and Figure 16). A plot of experimental $Q^1_{Q3}$ versus $Q^3$ concentration (Figure 15) was a convenient guide for construction of these representative species. For instance, in the $^{29}$Si NMR spectrum of R-0.9 sample recorded after 30 min, the $Q^1_{Q3}/Q^3$ ratio equaled 2. The smallest

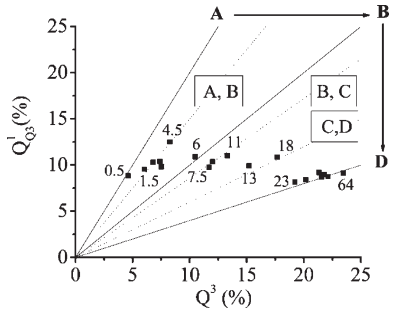


**Figure 15.** $Q^1_{Q3}$ vs $Q^3$ content of R-0.9 sample during its evolution. The figures next to the data points refer to the time (h). $Q^1_{Q3}/Q^3$ ratio's characteristic of model structures A−D shown in Figure 16 and Table 4 are represented with lines.

branched oligomer that can be formed involves the condensation between a dimer and the central Si atom of a trimer (molecule A in Figure 16, Table 4). This pentamer has two $Q^1_{Q3}$ groups and one $Q^3$. The 3D structure of this species is shown in Figure 17.

In the period between 0.5 and 20 h, hydrolyzed silicon atoms were observed at central positions of 4Si and 5Si chains (Figure 5). This period was characterized by the decrease of the content of dimer and trimer (Figure 13). Molecules B1 and B2 (Figure 16) are the result of condensation reactions between the end groups of trimer and the middle groups of tetramer and pentamer, respectively. In B1 and B2, the longest silica chain count six and seven Si atoms, respectively, explaining the experimental observation of an increasing number of such molecules (Figure 13). Similarly, reactions of end groups of dimers with middle groups of tetramers and pentamers will also lead to a branched specimen. A dominance of B type molecules in combination with some linear molecules can account for the $Q^n$ distribution observed at 6 h in R-0.9, viz., $Q^1_{Q3}$:$Q^1_{Q2}$:$Q^2$: $Q^3$ of 1:2.3:4:1 (Table 4). Molecules of type B presenting 1 branching have experimental $Q^1_{Q3}$ to $Q^3$ ratios of 1 (Figure 16), in excellent agreement with experimental observation (Figure 15 and Figure 13).

After 6 h, the content of dimer and trimer did not change any more (Figure 13). The content of 4Si and 5Si chains with a hydrolyzed $Q^2$ group continuously decreased in the period up to 20 h. Condensation reactions between these tetramers and pentamers and $Q^1_{Q2}$ and $Q^1_{Q3}$ groups of abundantly present molecules of type B led to type C molecules represented by molecules C1 and C2, respectively (Figure 16). The formation of molecules C presenting two branchings readily explained the observed decrease of the content of 4Si and 5Si chains in favor of 6Si and longer ($6Si^+$) chains (Figure 13).

After 20 h, almost no hydrolyzed $Q^2$ groups remained. $^{29}$Si NMR revealed a further gradual decrease of the content of $Q^1$ and $Q^2$ silicons in favor of $Q^3$ (Figure 2). These changes could be interpreted as a result of condensation reactions between type C molecules leading to heavier, even more branched structures D, examples of which are shown in Figure 16 (molecules D1 and D2). At the end of the experiment of R-0.9 (~57 h), most of the silicon was incorporated into structures of type D, whereof the $Q^1_{Q3}$:$Q^1_{Q2}$:$Q^2$:$Q^3$ ratio matches the experimental ratio of 0.4:0.7:1.7:1 (Table 4). Molecules of D are characterized by a $Q^1_{Q3}$ to $Q^3$ ratio of 0.5 (Figure 15). Model molecules A, B, and D represented key stages of the silica polycondensation obtained around 0.5, 6, and 57 h, respectively. In the plot of experimental

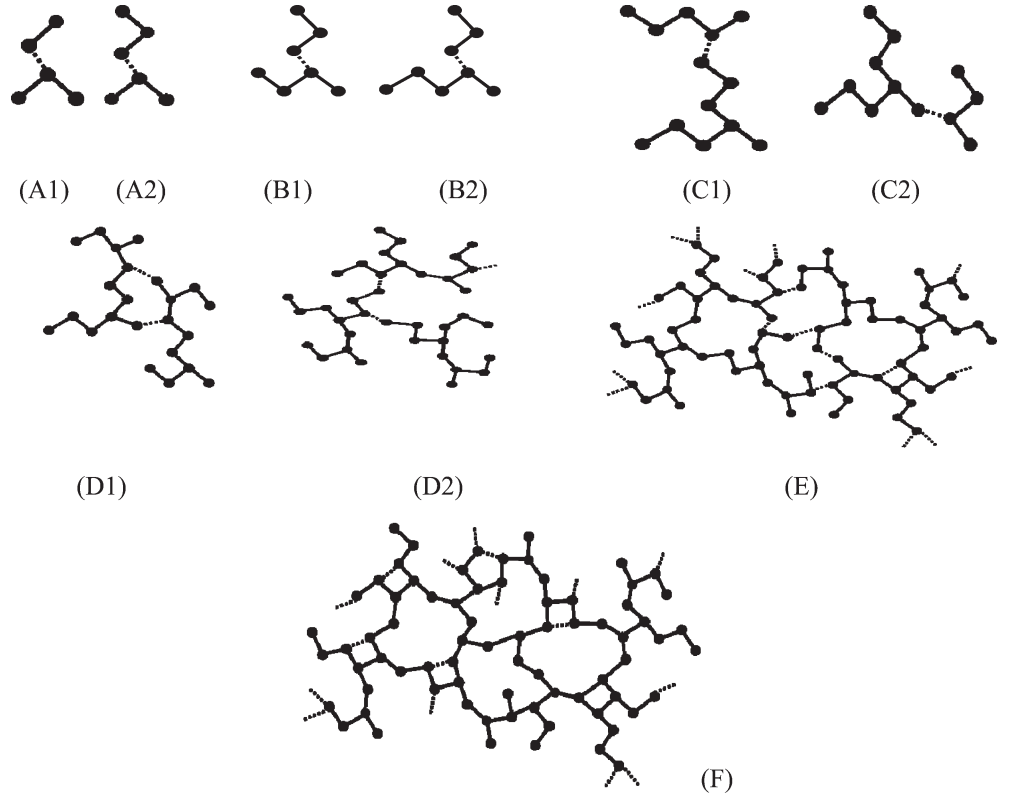


**Figure 16.** Condensation reactions (dotted lines) leading to the formation of representative molecules of the oligomerization process starting from TMOS under acid conditions and under stoichiometric water content (cf. Table 4).

$Q^1_{Q3}$ versus $Q^3$ content (Figure 15) the actual data points clearly highlighted the gradual transition from molecules A to D.

In the periods 0.5 and 6 h the $Q^1_{Q3}/Q^3$ ratio shifted from 2, characteristic of molecules of A, to 1, characteristic of molecules of B. Between 6 and 23 h, the experimental $Q^1_{Q3}/Q^3$ ratios corresponded to a silica speciation containing B and C. An almost pure C population was reached around 13 h, and around 23 h NMR indicated sole presence of species D. According to the $Q^1_{Q3}/Q^3$ ratio, little evolution in the molecular structure was observed later, between 23 and 64 h.

On the basis of this insight into the development of silicate network reached in the R-0.9 sample, the evolution of R-1.3 sample could also be understood. According to the $Q^n$ distribution sample R-1.3 was already at a further stage after 30 min compared to R-0.9 sample after 57 h (Table 4). With respect to $Q^3$ silicons, the content of $Q^1$ and $Q^2$ was already significantly lower, viz., 0.24 instead of 1.1 for $Q^1$ and 1.26 instead of 1.7 for $Q^2$ (Table 4). The $Q^n$ ratio of the R-1.3 sample could be simulated by subjecting molecules D to inter- and intramolecular reactions and generation of molecules of type E (Figure 16) having a $Q^1$:$Q^2$:$Q^3$ ratio of 0.3:1.2:1 in excellent agreement with the ratios (Table 4). The evolution of the $Q^n$ distribution of this sample (Figure 11) revealed that the evolution of the polymer involved mainly a transformation of $Q^2$ into $Q^3$ silicons. Intramolecular condensation of two $Q^2$ silicons of molecule E leads to molecule F, having $Q^1$:$Q^2$:$Q^3$ ratio of 0.2:0.6:1 matching with an experimental distribution observed at the final stage of this sample (Table 4).

These molecular models provided further insight into the Raman spectra. The Raman signal observed in R-1.3 sample around 550 $cm^{-1}$, a region originally assigned to isolated tetramers and trimers, originates from side chains of the polymer network represented in molecules E and F.

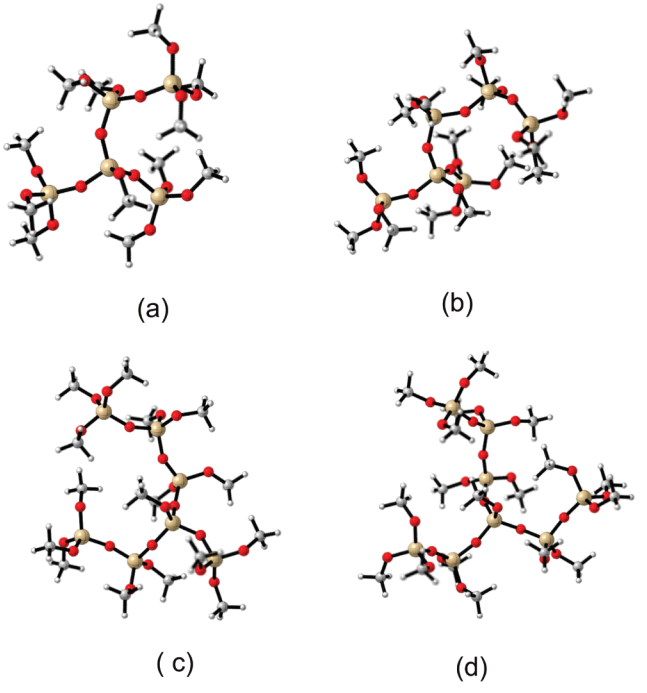


**Figure 17.** The lowest energy conformers of molecules A and B presented in Figure 16: A1 (a), A2 (b), B1 (c), and B2 (d).


dx.doi.org/10.1021/jp200568j |*J. Phys. Chem. C* 2011, 115, 11077–11088

**Scheme 1. Acid Catalyzed Silica Oligomerization Scheme Departing from TMOS[a]**

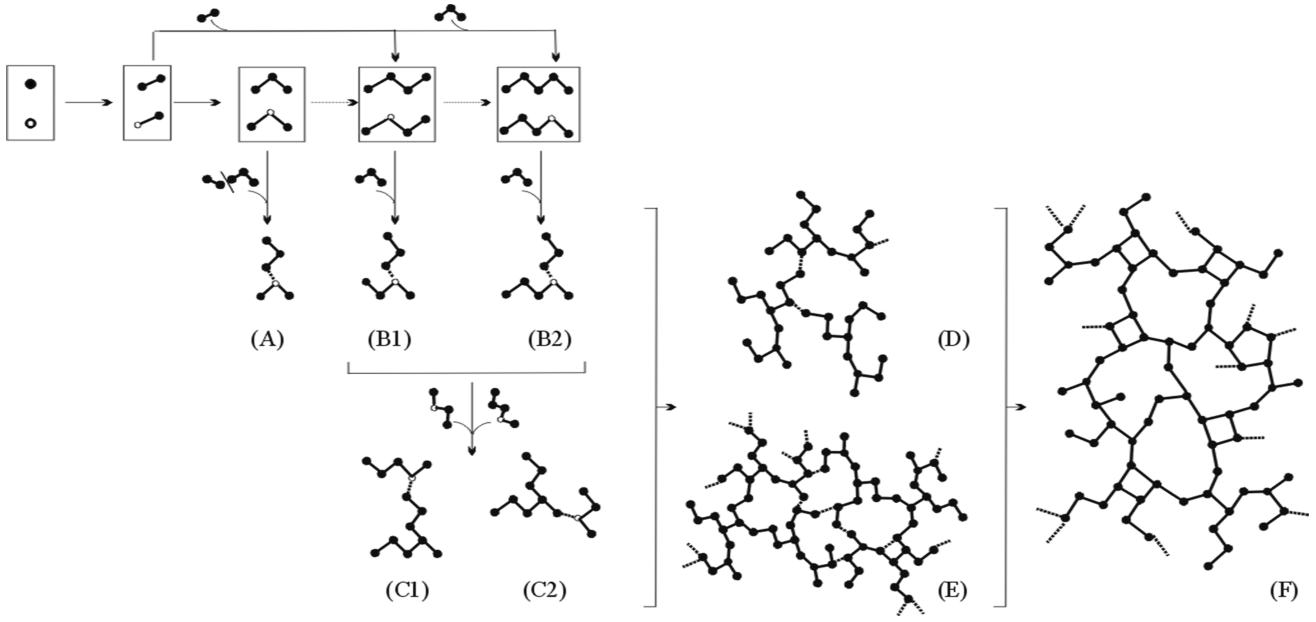


[a] Fully methoxide terminated and hydrolyzed silicon atoms are presented by solid (●) and open (○) dots, respectively.

Another intriguing aspect of this TMOS based sol−gel chemistry is the low tendency for formation of rings. According to the presented molecular structures A−F rings with four to six Si atoms are formed very late in the reaction network upon condensation of $Q^2$ silicons. The absence of $Q^2$ signals characteristic of cyclosilicates in the detailed NMR spectra of sample R-0.9 precluded the formation of rings in molecules A−D. Most likely, rings are formed with increasing number of intramolecular condensation reactions exemplified in molecules E and F. Note that these structures do not contain $Q^2$ silicon in their four-, five- and six-rings. In this model rings are almost entirely composed of $Q^3$ silicon.

The investigated samples did not evolve to the gel stage. Molecule E can already be thought of as a representative of the approached gel network. The presumed nature of the final gel network should then consist of a highly branched polymer, containing a limited amount of branched four-, five-, and six-rings. On the basis of our advanced analysis of the polymerization process, the here proposed final gel network shows striking similarities to the gel network proposed by Kelts and Armstrong for TMOS polymer grown at low pH.[49] The main difference between this work and that of Kelts and Armstrong is the absence of cylcosilicates as precursor units (Scheme 1). According to the presented observations, attachment of side chains is the main reaction pathway in TMOS based silica oligomerization. Surprisingly, this mechanism is significantly different from the reaction pathways observed in TEOS based silica oligomerization, where ring formation through cyclo-dimerization was recognized as important reaction pathway.[60] Steric and electronic factors most probably are at the origin of these differences.

The differences in polymerization pathways using TMOS and TEOS are expected to have an effect on the properties of the obtained silica gel. Departing from TMOS the gel network is characterized by a much higher branching degree and lower content of rings. The formation of microporous versus mesoporous silica gel depending on the use of TEOS versus TMOS[61] likely is due to these differences, but further research is needed to elucidate the details.

## CONCLUSIONS

A detailed analysis of NMR spectra and interpretation of silica speciation supported by UV-Raman spectroscopy and molecular modeling enabled us to propose a detailed reaction scheme (Scheme 1) of the conversion of TMOS into silica gel network under conditions of acid catalysis and low molar hydrolysis ratio. At an $r$ value of 0.9 TMOS readily hydrolyzed and oligomerized into short chains with three up to five Si atoms. Once most of the water was consumed, the condensations went slower. Residual hydrolyzed silicate groups were present almost exclusively at central positions of four and five Si chains. Characteristic stages of the building of the silica gel network could be identified and characteristic molecular structures were proposed (Figure 16). The condensations corresponded to an attachment of dimer and trimer to middle sections of short chains (molecules A and B, Figure 16). At the next stage tetramer and pentamer were attached via hydrolyzed middle groups to end groups (molecules C) until they were depleted. Intermolecular condensations via end and middle groups led to still larger structures D characterized by the absence of rings. A sample with $r$ value of 1.3 evolved much more rapidly and reached a further developed polymer structure already after 30 min. This sample had a highly branched silicate network lacking fully condensed silicon atoms and containing only a limited amount of four-, five-, and six-membered rings.

This paper adds to the assignment of both $^{29}$Si NMR and Raman signals. $^{29}$Si NMR signals at $\delta$ = −92.4, −92.72, −92.96, and −93.2 ppm were assigned to hydrolyzed $Q^2$ groups in chains of three, four, five, and six or more Si atoms, respectively. Signals at −93.61, −93.80, −94.01, and −94.26 ppm were assigned to fully methoxylated chains of four, five, and six or more Si atoms either isolated or part of a larger network. Distinction between $^{29}$Si NMR signals of $Q^1$ end groups next to $Q^2$ and $Q^3$ is revealed in NMR signatures at $\delta$ = −85.69 and −85.91, respectively. Raman signatures at ∼555, ∼540, and ∼510 cm$^{-1}$ were assigned to chains of three, four, five, and more Si atoms.

## ■ ASSOCIATED CONTENT

**Supporting Information.** Full *XYZ* coordinates of all optimized structures for the molecular modeling of Raman intensities, Raman frequencies, and $^{29}$Si NMR chemical shifts, correlation graphs for Raman and NMR scale factor determination, and complete ref 65. This material is available free of charge via the Internet at http://pubs.acs.org.

## ■ AUTHOR INFORMATION

**Corresponding Author**
*E-mail: Johan.Martens@biw.kuleuven.be.

## ■ ACKNOWLEDGMENT

A.D. acknowledges the Research Foundation Flanders (FWO) for a research fellowship. Theoretical work was supported by the Research Board of Ghent University (BOF) and BELSPO, through Interuniversity Attraction Poles (IAP-PAI P6/27). We greatly acknowledge Professor Tatjana Parac-Vogt and Karel Duerinckx for $^{29}$Si NMR measurements on a Bruker Avance II$^{+}$ 600 spectrometer (Center for Molecular Design and Synthesis at K.U. Leuven, Belgium). J.A.M. and C.E.A.K. acknowledge the Flemish Government for long-term structural funding (Methusalem), the Belgian Prodex office and ESA. V.V.S acknowledges the European Research Council under the European Community's Seventh Framework Programme (FP7 (2007-2013) ERC Grant Agreement Number 240483).

## ■ REFERENCES

(1) Rouse, J. H.; Ferguson, G. S. *J. Am. Chem. Soc.* **2003**, *125*, 15529.
(2) Shin, J. H.; Metzger, S. K.; Schoenfisch, M. H. *J. Am. Chem. Soc.* **2007**, *129*, 4612.
(3) Uemura, T.; Hiramatsu, D.; Yoshida, K.; Isoda, S.; Kitagawa, S. *J. Am. Chem. Soc.* **2008**, *130*, 9216.
(4) Wang, J.; Pamidi, P. V. A.; Zanette, D. R. *J. Am. Chem. Soc.* **1998**, *120*, 5852.
(5) Livage, J. *Chem. Mag. (Den Haag)* **1990**, 67.
(6) Livage, J.; Babonneau, F.; Sanchez, C. *Sol-gel optics*; Kluwer Pub., 1994.
(7) Livage, J.; Ganguli, D. *Sol. Energy Mater. Sol. Cells* **2001**, *68*, 365.
(8) Aelion, R.; Loebel, A.; Eirich, F. *J. Am. Chem. Soc.* **1950**, *72*, 5705.
(9) Assink, R. A.; Kay, B. D. *J. Non-Cryst. Solids* **1988**, *99*, 359.
(10) Bernards, T. N. M.; Vanbommel, M. J.; Boonstra, A. H. *J. Non-Cryst. Solids* **1991**, *134*, 1.
(11) Bertoluzza, A.; Fagnano, C.; Antonietta Morelli, M.; Gottardi, V.; Guglielmi, M. *J. Non-Cryst. Solids* **1982**, *48*, 117.
(12) Brinker, C.; Scherer, G. *Sol-Gel Science: The Physics and Chemistry of Sol-Gel Processing*; Academic Press: Boston, MA, 1990.
(13) Colomban, P. *J. Raman Spectrosc.* **1996**, *27*, 747.
(14) James, P. F. *J. Non-Cryst. Solids* **1988**, *100*, 93.
(15) Lin, C. C.; Basil, J. D. *Mater. Res. Soc. Symp. Proc.* **1986**, *73*, 585.
(16) Matsuyama, I.; Satoh, S.; Katsumoto, M.; Susa, K. *J. Non-Cryst. Solids* **1991**, *135*, 22.
(17) Mulder, C. A. M.; Damen, A. *J. Non-Cryst. Solids* **1987**, *93*, 169.
(18) Pouxviel, J. C.; Boilot, J. P.; Beloeil, J. C.; Lallemand, J. Y. *J. Non-Cryst. Solids* **1987**, *89*, 345.
(19) Livage, J. *Stud. Surf. Sci. Catal.* **1994**, *85*, 1.
(20) Aegerter, M. A.; Mennig, M. *Sol-gel technologies for glass producers and users*; Kluwer Academic Publishers: Boston, MA, 2004.
(21) Livage, J.; Beteille, F.; Roux, C.; Chatry, M.; Davidson, P. *Acta Mater.* **1998**, *46*, 743.
(22) Livage, J.; Sanchez, C. *J. Non-Cryst. Solids* **1992**, *145*, 11.
(23) Nabavi, M.; Doeuff, S.; Sanchez, C.; Livage, J. *J. Non-Cryst. Solids* **1990**, *121*, 31.
(24) Artaki, I.; Bradley, M.; Zerda, T. W.; Jonas, J. *J. Phys. Chem.* **1985**, *89*, 4399.
(25) Brinker, C. J.; Keefer, K. D.; Schaefer, D. W.; Ashley, C. S. *J. Non-Cryst. Solids* **1982**, *48*, 47.
(26) Petry, D. P.; Haouas, M.; Wong, S. C. C.; Aerts, A.; Kirschhock, C. E. A.; Martens, J. A.; Gaskell, S. J.; Anderson, M. W.; Taulelle, F. *J. Phys. Chem. C* **2006**, *113*, 20827–20836.
(27) Marino, I.-G.; Lottici, P. P.; Bersani, D.; Raschellà, R.; Lorenzi, A.; Montenero, A. *J. Non-Cryst. Solids* **2005**, *351*, 495.
(28) Mora-Fonz, M. J.; Catlow, C. R. A.; Lewis, D. W. *J. Phys. Chem. C* **2007**, *111*, 18155.
(29) Trinh, T. T.; Jansen, A. P. J.; van Santen, R. A. *J. Phys. Chem. B* **2006**, *110*, 23099.
(30) Zerda, T. W.; Artaki, I.; Jonas, J. *J. Non-Cryst. Solids* **1986**, *81*, 365.
(31) Yu, Y.; Xiong, G.; Li, C.; Xiao, F.-S. *J. Catal.* **2000**, *194*, 487.
(32) Dutta, P. K.; Shieh, D. C.; Puri, M. *Zeolites* **1988**, *8*, 306.
(33) Knops-Gerrits, P.-P.; De Vos, D. E.; Feijen, E. J. P.; Jacobs, P. A. *Microporous Mater.* **1997**, *8*, 3.
(34) Dutta, P. K.; Rao, K. M.; Park, J. Y. *J. Phys. Chem.* **1991**, *95*, 6654.
(35) De Man, A. J. M.; Van Santen, R. A. *Zeolites* **1992**, *12*, 269.
(36) Russel, P. E. *Microbeam analysis*; San Fransisco Press: San Fransisco, CA, 1989.
(37) Bornhauser, P.; Bougeard, D. *J. Raman Spectrosc.* **2001**, *32*, 279.
(38) Mozgawa, W. *J. Mol. Struct.* **2001**, *596*, 129.
(39) Dutta, P. K.; Del Barco, B. *J. Phys. Chem.* **1985**, *89*, 1861.
(40) Dutta, P. K.; Del Barco, B. *J. Phys. Chem.* **1988**, *92*, 354.
(41) Dutta, P. K.; Twu, J. *J. Phys. Chem.* **1991**, *95*, 2498.
(42) Bremard, C.; Le Maire, M. *J. Phys. Chem.* **1993**, *97*, 9695.
(43) Mozgawa, W.; Bajda, T. *J. Mol. Struct.* **2006**, *792−793*, 170.
(44) Mozgawa, W.; Jastrzebski, W.; Handke, M. *J. Mol. Struct.* **2006**, *792−793*, 163.
(45) Krause, K.; Geidel, E.; Kindler, J.; Förster, H.; Smirnov, K. S. *Vib. Spectrosc.* **1996**, *12*, 45.
(46) Pavel, C. C.; Zibrowius, B.; Loffler, E.; Schmidt, W. *Phys. Chem. Chem. Phys.* **2007**, *9*, 3440.
(47) Brinker, C. J.; Assink, R. A. *J. Non-Cryst. Solids* **1989**, *111*, 48.
(48) Brunet, F.; Cabane, B. *J. Non-Cryst. Solids* **1993**, *163*, 211.
(49) Kelts, L. W.; Armstrong, N. J. *J. Mater. Res.* **1989**, *4*, 423.
(50) Kelts, L. W.; Effinger, N. J.; Melpolder, S. M. *J. Non-Cryst. Solids* **1986**, *83*, 353.
(51) Lippert, J. L.; Melpolder, S. B.; Kelts, L. M. *J. Non-Cryst. Solids* **1988**, *104*, 139.
(52) Bailey, J. K.; Macosko, C. W.; Mecartney, M. L. *J. Non-Cryst. Solids* **1990**, *125*, 208.
(53) Brus, J.; Karhan, J.; Kotlik, P. *Collect. Czech. Chem. Commun.* **1996**, *61*, 691.
(54) Balfe, C. A.; Martinez, S. L. *Mater. Res. Soc. Symp. Proc.* **1986**, *73*, 27.
(55) Engelhardt, G.; Michel, D. *High-resolution solid-state NMR of silicates and zeolites*; John Wiley and Sons Ltd.: Chichester and New York, 1987.
(56) Klemperer, W. G.; Ramamurthi, S. D. *J. Non-Cryst. Solids* **1990**, *121*, 16.
(57) Ng, L. V.; Thompson, P.; Sanchez, J.; Macosko, C. W.; McCormick, A. V. *Macromolecules* **1995**, *28*, 6471.
(58) Sanchez, J.; McCormick, A. *J. Phys. Chem.* **1992**, *96*, 8973.
(59) Pienaar, C. L.; Chiffoleau, G. J. A.; Follens, L. R. A.; Martens, J. A.; Kirschhock, C. E. A.; Steinberg, T. A. *Chem. Mater.* **2007**, *19*, 660.
(60) Depla, A.; Lesthaeghe, D.; van Erp, T. S.; Aerts, A.; Houthoofd, K.; Fan, F.; Li, C.; Van Speybroeck, V.; Waroquier, M.; Kirschhock, C. E. A.; Martens, J. A. *J. Phys. Chem. C* **2011**accepted.
(61) Depla, A.; Kirschhock, C.; Martens, J. *Stud. Surf. Sci. Catal.* **2010**, *175*, 801.

(62) Maier, W. F.; Tilgner, I. C.; Wiedorn, M.; Ko, H. C. *Adv. Mater.* **1993**, *5*, 726.
(63) Lazzeri, M.; Mauri, F. *Phys. Rev. Lett.* **2003**, 90.
(64) Casanovas, J.; Illas, F.; Pacchioni, G. *Chem. Phys. Lett.* **2000**, *326*, 523.
(65) Frisch, M. J.; et al. *Gaussian 03*; Gaussian, Inc.: Wallingford, CT, 2003 (For complete list of authors, see Supporting Information).
(66) Van Houteghem, M.; Verstraelen, T.; Van Neck, D.; Kirschhock, C. E. A.; Martens, J. A.; Waroquier, M.; Van Speybroeck, V. *J. Chem. Theory Comput.* **2011**, *7*, 1045.
(67) Becke, A. D. *J. Chem. Phys.* **1993**, *98*, 5648.
(68) Merrick, J. P.; Moran, D.; Radom, L. *J. Phys. Chem. A* **2007**, *111*, 11683.
(69) Sykes, D.; Kubicki, J. D.; Farrar, T. C. *J. Phys. Chem. A* **1997**, *101*, 2715.
(70) Mennucci, B.; Martinez, J. M.; Tomasi, J. *J. Phys. Chem. A* **2001**, *105*, 7287.
(71) Cho, H.; Felmy, A. R.; Craciun, R.; Keenum, J. P.; Shah, N.; Dixon, D. A. *J. Am. Chem. Soc.* **2006**, *128*, 2324.
(72) Butler, K.; Slater, B.; Lewis, D. W. *Zeolites and Related Materials: Trends, Targets and Challenges: Proceedings of the 4th International FEZA Conference*; Studies in surface science and catalysis 174; Elsevier: Amsterdam and London, 2008; p 725.
(73) Moravetski, V.; Hill, J. R.; Eichler, U.; Cheetham, A. K.; Sauer, J. *J. Am. Chem. Soc.* **1996**, *118*, 13015.
(74) Van Speybroeck, V.; Moonen, K.; Hemelsoet, K.; Stevens, C. V.; Waroquier, M. *J. Am. Chem. Soc.* **2006**, *128*, 8468.
(75) Verstraelen, T.; Szyja, B. M.; Lesthaeghe, D.; Declerck, R.; Van Speybroeck, V.; Waroquier, M.; Jansen, A. P. J.; Aerts, A.; Follens, L. R. A.; Martens, J. A.; Kirschhock, C. E. A.; van Santen, R. A. *Top. Catal.* **2009**, *52*, 1261.
(76) Brunet, F.; Cabane, B.; Dubois, M.; Perly, B. *J. Phys. Chem.* **1991**, *95*, 945.
(77) Gnado, J.; Dhamelincourt, P.; Pelegris, C.; Traisnel, M.; Mayot, A. L. *J. Non-Cryst. Solids* **1996**, *208*, 247.
(78) Matos, M. C.; Ilharco, L. M.; Almeida, R. M. *J. Non-Cryst. Solids* **1992**, *147−148*, 232.